Electrical Power and Energy Systems 155 (2024) 109672

Contents lists available at ScienceDirect

International Journal of Electrical Power and Energy Systems

journal homepage: www.elsevier.com/locate/ijepes

Integrated simulation of electromechanical and thermal dynamics of voltage source converters

Juan Manuel Mauricio, J. Carlos Olives-Camps, José María Maza-Ortega *, Antonio Gómez-Expósito

Department of Electrical Engineering, Universidad de Sevilla, Camino de los descubrimientos s/n, Seville, 41092, Spain

ARTICLE INFO

Keywords:
Insulated-gate bipolar transistors (IGBTs)
Junction temperature consideration
Power system simulation
Thermal modeling
Two-level voltage source converter (VSC)

ABSTRACT

This paper proposes a simplified yet accurate enough thermal model of Voltage Source Converters (VSC), aimed at circumventing the high computational cost of existing models, which prevents their use in electromechanical simulations. The proposed model reduces to a simple first-order system for thermal dynamics plus two quadratic equations separately modeling the IGBT and diode power losses. In addition, a methodology is provided to derive the proposed VSC thermal model parameters from manufacturer data. The proposed model is tested for two types of devices, both in steady and transient states. The results show that the reduced-order thermal model produces accurate results at a low computational cost, making it especially suitable for the co-simulation of thermal and electrical dynamic phenomena.

1. Introduction

The proliferation of Voltage Source Converters (VSCs) in power systems is unstoppable. VSCs are interfacing renewable energy sources (photovoltaic and wind energy systems), storage units (supercapacitors, batteries and flywheels), railway systems and they are also present in High Voltage DC (HVDC) and Flexible AC Transmission Systems (FACTS) applications [1]. The semiconductor switches most commonly used in VSC applications are the insulated-gate bipolar transistors (IGBTs). One of the main limitations of semiconductor switches, determining their safe operating area, refers to the maximum junction temperature, which evolves in accordance to power losses and the design of the thermal dissipator. Commonly, this temperature is limited to values around 125 or 150 °C for IGBTs. Exceeding this thermal limit reduces the IGBT useful life and may cause irreversible damages. For this reason, manufacturers offer data about the maximum currents for some operating conditions, usually in steady-state regime, and transient overloads over a short time, supposedly guaranteeing a junction temperature below its maximum value. However, such maximum currents stand just for those standardized conditions. Therefore, it is of utmost importance to develop a simulation tool capable of dealing with the thermal behavior (power losses, heat dissipation and IGBT temperature) of power electronics devices under any circumstances, particularly nowadays, when traditional synchronous machines are being replaced by power converters [2], which are called to provide flexibility in order to keep the network operating in a stable manner. As a matter of fact, this is already regulated on the generation side by restrictive grid codes [3,4], where renewable power plants are no longer expected to operate as pure active power injections with unity power factor. These specifications force power converters to offer similar ancillary services to those provided by classical synchronous generators. Reactive power support [5,6], inertia provision [7,8], frequency regulation [9], ramp limitation [10,11] are some of these ancillary services. An adequate computational tool including an accurate thermal model may disclose relevant information about how these ancillary services can be provided, possibly allowing transient overloads above the steady-state limits, but also about their impact on the device, i.e. additional power losses and thermal stress.

Such simulation tool must take into account the different dynamics involved in the thermal and electrical parts of the power electronics device. Fig. 1 shows different power system phenomena and their associated time constants. Those transients that are considered fast (from 1 μs to some few seconds) are within the electromagnetic domain while those slower than 1 ms are considered in the electromechanical one. The reduced time steps required for simulating electromagnetic phenomena prevent simulations of more than a dozen generators or so, as CPU times would be unacceptable otherwise. On the contrary, electromechanical simulations may tackle with thousands of them at reasonable computational cost. Note that most of the ancillary services mentioned above fall within this slow dynamic range and, therefore, they are analyzed through electromechanical simulations.

* Corresponding author.
E-mail address: jmmaza@us.es (J.M. Maza-Ortega).

https://doi.org/10.1016/j.ijepes.2023.109672
Received 8 November 2022; Received in revised form 24 September 2023; Accepted 16 November 2023
Available online 23 November 2023

Nomenclature

I	RMS current
$\underline{I} = Ie^{j\theta}$	Phasor current
$\underline{V}_s = V_s e^{j\theta_s}$ and $\underline{V}_t = V_t e^{j\theta_t}$	Phasor phase-to-neutral grid and VSC voltage
V_{ac}	AC phase-to-phase RMS grid voltage
φ	Power factor angle
P_i and P_d	Individual IGBT and diode power losses
P_s	Single switch (IGBT and diode) power losses
T_a	Ambient temperature
T_i and T_d	IGBT and diode juncture temperature
T_c and T_s	Case and heatsink temperature
T_s^{ss}	Heatsink steady-state temperature
N_h	Number of heatsink switches
R_{th}^{i-s}	IGBT juncture-to-heatsink thermal resistance
R_{th}^{d-s}	Diode juncture-to-heatsink thermal resistance
R_{th}^{s-a}	Heatsink-to-ambient thermal resistance
C_{th}^{s}	Heatsink thermal capacitance

The issue is that thermal analysis of IGBT-based switches is a complex task, because some phenomena belong to the electromagnetic domain, e.g. IGBT juncture and case time constant ($\tau < 100$ ms), while others are in the slower range of the electromechanical domain, e.g. heatsink temperature time constant ($\tau > 10$ s). Several accurate electrothermal models for IGBTs are described and implemented in [12–17]. However the scope of those models is the very fast thermal transient of the juncture temperature. Such models require considering the physics involved in the switching process to determine the switching and conduction losses. This kind of model is typically developed on electromagnetic simulations platforms, such as SPICE, SABER or EMTP, requiring integration time steps smaller than 1 μs [18]. A model simplification is proposed in [19], where the overall thermal model is overly reduced to just one differential equation. However, this equation retains the small time constant of the original model and, therefore, it requires the use of reduced time steps for practical purposes.

In addition to modeling the thermal behavior of the VSC, another major issue is that of finding suitable values for the involved model parameters. Semiconductor manufacturers provide software tools for this purpose, but most of them are on-line tools [20–24], hindering the interaction between the electric and thermal simulations. Those tools provide a simulation environment to analyze whether the power electronic switch is able to withstand a given load profile, usually defined as a steady-state load with an overload factor during a long period of time, which is totally unsuitable for the framework of electromechanical studies.

Considering the above issues, this paper proposes an original methodology to incorporate the thermal behavior of power electronic devices in electromechanical simulations. For this purpose, a new thermal domain, as depicted in blue in Fig. 1, is defined. The time scale range associated to this new domain is able to consider the most important transients from the point of view of the electromechanical model, while simplifying the fast thermal dynamic complexity. For doing so, the approach considered in [25] is adopted, by which fast dynamics, e.g. fast thermal junction and case thermal phenomena, are modeled as algebraic equations while slow dynamics, e.g. heatsink behavior, are represented by differential ones. Moreover, the model parameters can be computed in a straightforward manner from public data provided by the semiconductor manufacturers. In this way, the parameterized thermal model can be easily integrated into electromechanical simulations, facilitating the analysis of the thermal behavior and limitations of power electronics converters.

The rest of the paper is organized as follows. Section 2 provides the methodology proposed in this paper for the integrated analysis of electromechanical and thermal simulation of VSCs. Section 3 presents a mathematical model of the power losses generated in the operation of power switches and the thermal model describing the heat transfer. In the same section, a method to obtain the constants that appear in these models is detailed. The implementation of the proposed thermal model in current VSC electromechanical models is explained in Section 4. Section 5 validates the proposed thermal model by comparing its results with the manufacturer solutions. Finally, the document closes with the conclusions.

2. Proposed methodology

As the thermal and electromechanical simulation tools are implemented in separate software platforms, power engineers dealing with these issues necessarily follow the workflow depicted on the top diagram of Fig. 2. The first step is to perform dynamic network studies with electromechanical simulation programs, e.g. PSS/E or DigSILENT, where the device under study is faced to the worst scenario conditions. After that, the required input information for the thermal analysis tool must be extracted from the simulated data and exported to the manufacturer application. Usually this corresponds to a reduced time series of VSC RMS current, power factor and modulation index, whose size mainly depends on the manufacturer software characteristics. Then, the thermal behavior is simulated, yielding typically information about temperatures and power losses. If the temperature exceeds the imposed limits, the designer has to run again the electromechanical simulation with new limits or a different control strategy. Therefore, the current methodology is a tedious iterative process involving data transfers back and forth between separate simulation tools.

The proposed methodology can be explained with the help of the bottom diagram of Fig. 2. Basically, it relies on obtaining a thermal model from the manufacturer simulation tool and incorporating it within the electromechanical simulation. This greatly simplifies the process for three reasons. First, for a given power electronic stack, it is required to obtain the thermal model only once by using the manufacturer simulation tool. Second, power losses and temperatures are obtained in a straightforward manner from the power system simulation tool, just by incorporating the tuned thermal model. Third, as the temperature variable is explicitly handled within the electromechanical simulation, it should be possible to incorporate additional constraints, such as temperature protections or even controllers that consider the temperature evolution, which is very awkward to do using existing models.

3. VSC thermal model

This section presents the thermal model required to obtain the different operating temperatures of a VSC. The section is subdivided into three different subsections dealing respectively with the VSC thermal dynamic model, which relates temperatures with the heat sources, the power losses model and a method for computing all the model parameters using available data from manufacturers.

It is worth noting that the proposed VSC thermal model relies on simulation tools provided by manufacturers. It is assumed that these thermal simulation tools have been previously validated by the manufacturers through experimental testing, given the fact that they are widely used to rate and design the power electronic stacks. For this reason, the experimental validation of the proposed thermal model is out of the scope of this paper.

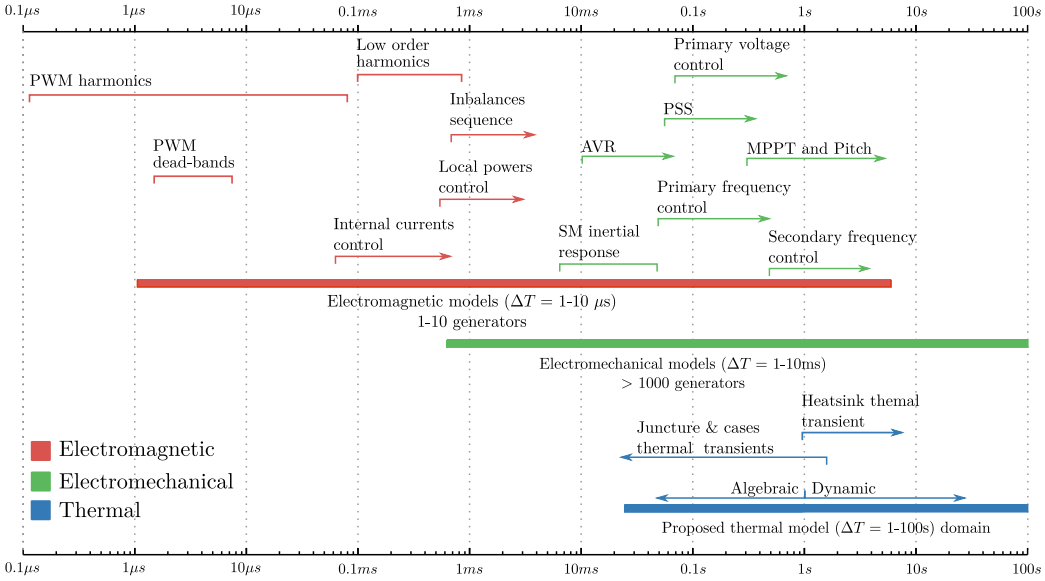

Fig. 1. Time scale of dynamic phenomena in power systems and their relationship with simulation domains.

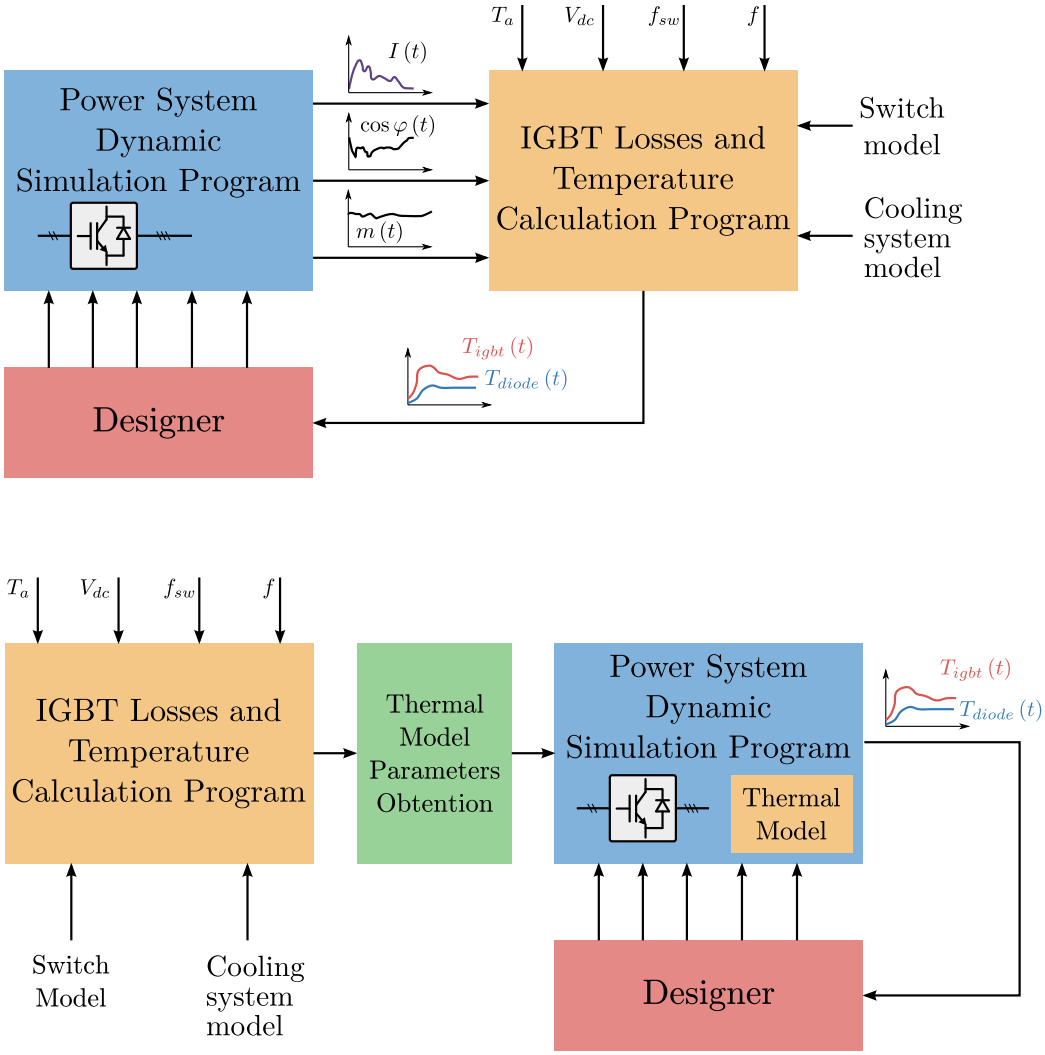

Fig. 2. Methodologies for assessing the thermal behavior of VSC in electromechanical simulations. Top diagram: current iterative method. Bottom diagram: proposed integrated or joint approach.

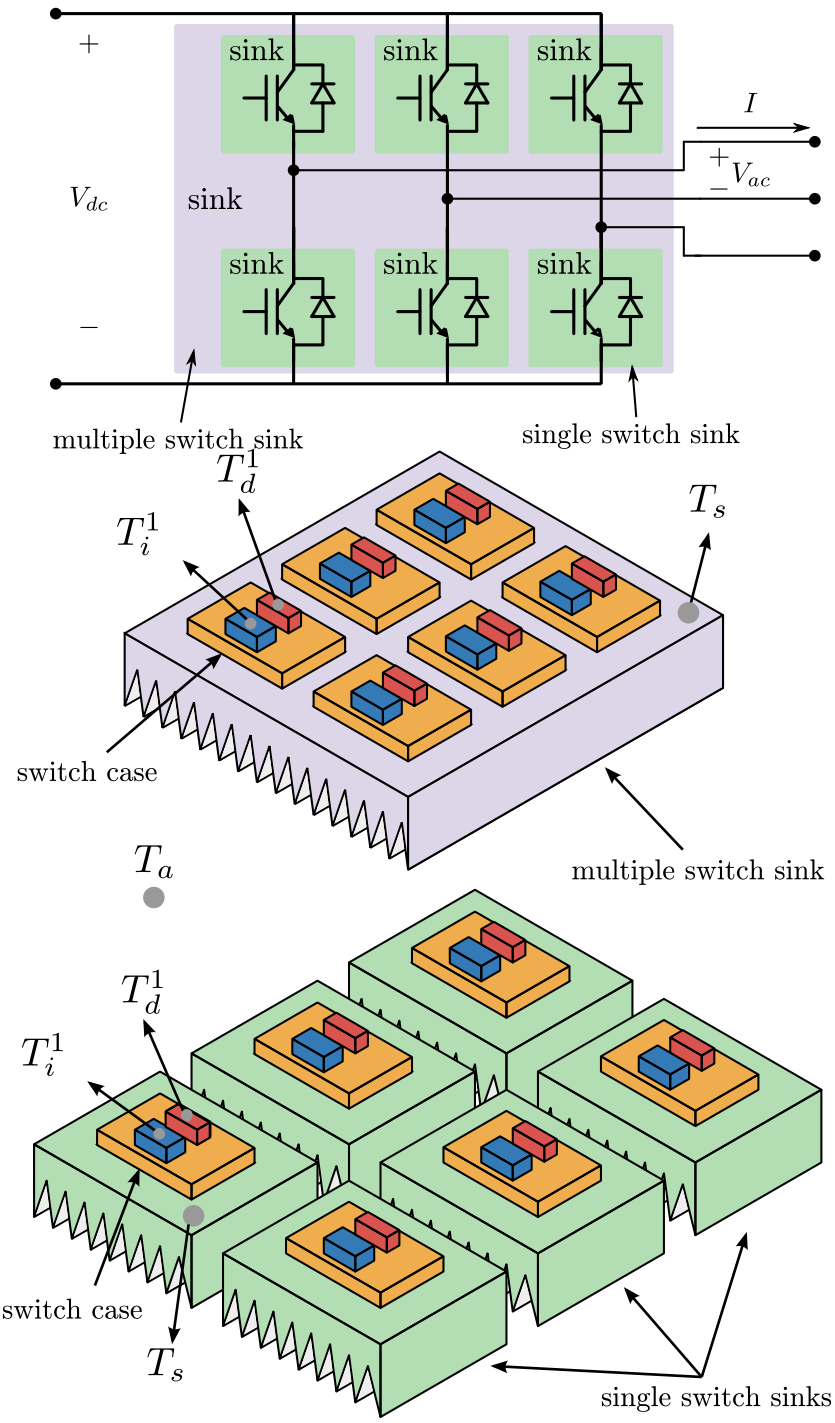

Fig. 3. VSC circuit and physical VSC schemes with different heatsink arrangements.

3.1. VSC thermal dynamics

This subsection describes the model representing the VSC thermal behavior, assuming that the only heat source corresponds to the power losses of the semiconductor devices, to be analyzed in the next subsection. It is considered that any switch is composed of an IGBT and its corresponding anti-parallel diode, as shown on the top of Fig. 3. It will be also assumed that N_h switches are installed on a single heatsink. Note that N_h does not represent the total number of switches of the power electronic stack, but just those sharing the same heatsink. According to this, $N_h = 6$ and $N_h = 1$ for the configurations shown in the middle and lower schemes of Fig. 3, respectively. In case of power stacks with several heatsinks, no thermal interaction between them will be assumed.

The objective of the thermal model is to determine how the power losses are dissipated from the semiconductor switches to the environment. Considering the involved elements illustrated in Fig. 3, the resulting heat transfer can be split into three different parts: (i) from the IGBT/diode junction to the corresponding case; (ii) from the IGBT/diode case to the heatsink; (iii) from the heatsink to the environment.

Usually, the thermal model is represented by using an analogy with an electric equivalent circuit, as proposed by Cauer [26,27]. In this analogy, the heat generators are current sources while the environment

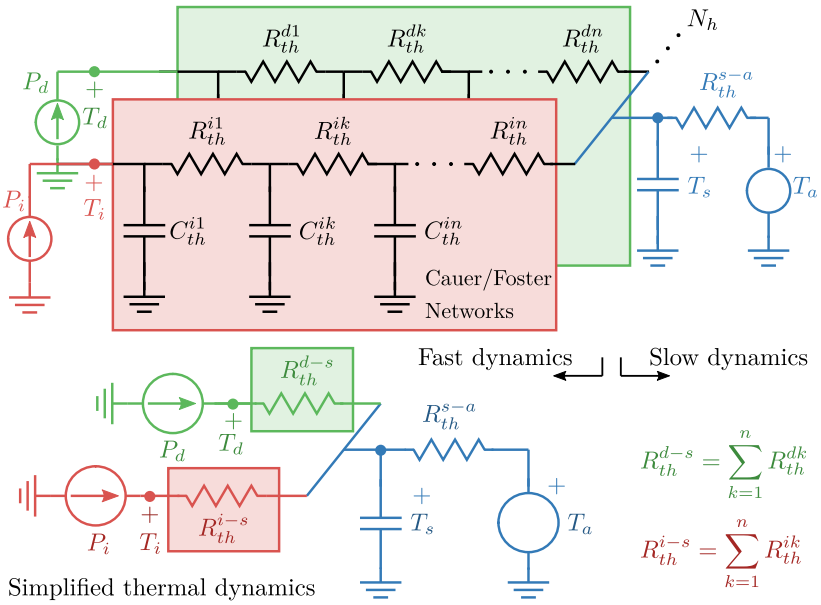

Fig. 4. Cauer thermal model of the heatsink with semiconductor switches and simplified model.

with a constant temperature is represented as a voltage source [21]. Between these two extremes, from the heat source to the environment, the thermal dynamic behavior of the different elements involved in the heat flow is represented using multiple pairs of resistors and capacitors. The capacitor voltages represents the different element temperatures, which are state variables of the dynamic problem. Fig. 4 shows the derived electric circuit of the thermal model, comprising N_h power electronic switches with a common heatsink where only one switch, composed of an IGBT and diode, is depicted.

A detailed analysis of the internal thermal dynamics corresponding to the IGBT/diode junction-case and case-heatsink reveals that it is really fast, with time constants of just a few milliseconds [20]. Therefore, in the thermal domain illustrated in Fig. 4, this fast process can be reduced to an algebraic equation, converting temperatures from state variables to algebraic quantities. It is important to point out that this simplification does not eliminate the faster temperature dynamics. The transformation into an algebraic relationship simply yields a discrete temperature evolution up to the steady-state condition. Moreover, this simplification offers conservative results, because any sudden change in the boundary conditions, e.g. power losses or environment temperature, may cause a smooth evolution of the actual temperature whereas the simulated one varies stepwise. Note that this simplification implies eliminating the capacitors of the equivalent circuit, as shown in the bottom diagram of Fig. 4. Therefore, and assuming the same power losses for the N_h switches, the thermal model accounting for the variation of the IGBT and diode temperature as a function of the heatsink temperature can be easily derived:

$$T_i = T_s + P_i R_{th}^{i-s}, \tag{1}$$

$$T_d = T_s + P_d R_{th}^{d-s}. \tag{2}$$

It is worth noting that this part of the thermal model neglects the thermal cross-coupling between the IGBT and diode [28], an information which, in any case, is not currently included in the manufacturers' data sheets. However, the proposed methodology could be easily updated to consider this effect just by adding the corresponding cross-coupling thermal resistors to the thermal model shown in Fig. 4.

Conversely, the dynamics of the heatsink temperature are within the time frame analyzed in the electromechanical simulations and, therefore, according to Fig. 4, can be modeled as:

$$\frac{dT_s}{dt} = \frac{1}{C_{th}^s}\left(N_h P_s - \frac{T_s - T_a}{R_{th}^{s-a}}\right) \tag{3}$$

where $P_s = P_i + P_d$ represents the sum of IGBT and diode power losses. The heatsink steady-state temperature, T_{ss}^s, can be obtained by forcing the left side of (3) to zero:

$$T_s^{ss} = T_a + R_{th}^{s-a} N_h P_s. \tag{4}$$

Then, it is possible to compute the normalized heatsink temperature, defined as $\Theta = T_s/T_s^{ss}$, which will be used to estimate precisely the IGBT and diode power losses, as explained in the next subsection. According to its definition, this variable is equal to one in the steady-state case, and can be considered almost constant for most studies. However, it must be taken into account in case a precise analysis of the thermal dynamics is required.

3.2. Power losses model

The power losses depend on a wide variety of factors such as the AC currents, AC and DC side voltages, switching frequency, ambient temperature, gate resistors, etc. Some of these variables can vary over a wide range depending on operating conditions of the grid-connected VSC, particularly:

1. AC RMS injected currents.
2. Power factor.
3. AC RMS grid voltages, which may also vary widely if the VSC has to operate under short-circuit conditions.

On the contrary, it is reasonable to consider that the following variables are almost constant:

1. Switching frequency is almost constant due to the use of PWM strategies.
2. DC voltage is constant because of the use of a proper DC regulator.
3. Ambient temperature remains constant. This is a feasible hypothesis considering the usual simulation intervals or, moreover, considering that the large power electronic stacks are within cabinets with controlled ambient temperature by means of Heat, Ventilation and Air Conditioning (HVAC) systems.

Those assumptions simplify to a greater extent the complexity of the power losses model and are fully feasible considering conventional engineering implementation of power electronic devices.

With the above considerations, it is possible to formulate the IGBT and diode power losses as follows:

$$P_i(I,\alpha) = \Theta\left(a_i + \left(b_i + c_i\alpha\right) I + \left(d_i + e_i\alpha\right) I^2\right) \tag{5}$$

$$P_d(I,\alpha) = \Theta\left(a_d + \left(b_d + c_d\alpha\right) I + \left(d_d + e_d\alpha\right) I^2\right) \tag{6}$$

where I is the VSC AC injected current, Θ is the normalized heatsink temperature and α is the product of the VSC modulation index, m, and power factor, $\cos\varphi$. Basically, the model is composed of two factors: the steady-state power losses and a correction term which takes into account the dependence of the power losses with the dynamic evolution of the temperature.

The first factor computes the IGBT/diode power losses depending on electrical variables at steady-state conditions. Therefore, the influence of the steady-state temperature is inherently considered in the IGBT/diode power losses. This factor depends on quadratic functions of some electrical variables (RMS current, modulation index and the power factor) whose coefficients (a_x, b_x, c_x, d_x and e_x where $x = i, d$) must be conveniently adjusted to accurately represent the off-state blocking, conduction and switching losses of electronic power devices.

The second factor corrects the IGBT/diode power losses considering the dynamic evolution of the temperature. Note that the higher the temperature the higher the losses. Therefore, it is proposed to model this dependence in a linear fashion by introducing the normalized heatsink temperature parameter Θ. This way, given that the heatsink temperature is a state variable in the thermal model, it is possible to accurately represent the transient variation of IGBT/diode power losses.

3.3. Estimation of thermal model parameters

This subsection is devoted to define the procedure for obtaining all the parameters of the thermal and power losses models.

Regarding the thermal model, it is required to determine the involved thermal resistors and capacitors of (1), (2) and (3), as shown in Fig. 4. Particularly, R_{th}^{i-s} and R_{th}^{d-s} are directly provided by manufacturers or derived from related data, such as the junction, T_i^{ss} or T_d^{ss}, and heatsink temperatures, T_s^{ss}, in steady-state conditions for a given scenario with power losses, P_i or P_d:

$$R_{th}^{i-s} = \frac{T_i^{ss} - T_s^{ss}}{P_i},$$

$$R_{th}^{d-s} = \frac{T_d^{ss} - T_s^{ss}}{P_d}.$$

Similarly, R_{th}^{s-a} can be determined as:

$$R_{th}^{s-a} = \frac{T_s^{ss} - T_a}{P_i + P_d}.$$

The thermal capacitor is obtained from the manufacturers' software through the simulation of a step change on the AC RMS current, which will cause a temperature evolution as shown in Fig. 5. This exponential curve allows to compute the time constant of the thermal capacitance as follows:

$$\tau_s = R_{th}^{s-a} C_{th}^{s} \Rightarrow C_{th}^{s} = \frac{\tau_s}{R_{th}^{s-a}}, \tag{7}$$

Regarding the parameters of the power losses model, according to (5) and (6), it is required to obtain ten parameters: a_x, b_x, c_x, d_x and e_x where $x = \{i, d\}$. Given the fact that the power losses depend linearly on these parameters, a straightforward procedure consists of evaluating (5) and (6) for n operating points characterized by different I_j and α_j with $j = 1, \ldots, n$ and $n \geq 5$. This can be formulated in matrix form as follows:

$$\mathbf{A}\mathbf{y}_\mathbf{x} = \mathbf{b}_\mathbf{x} \quad x = \{i, d\} \tag{8}$$

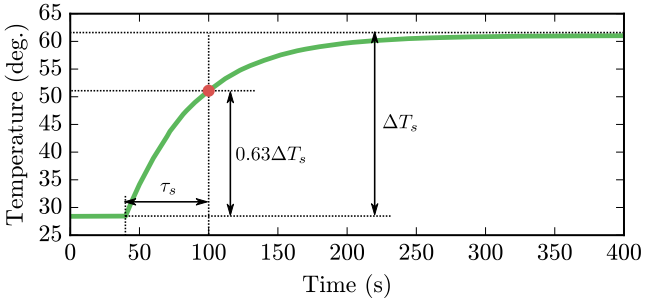

Fig. 5. Dynamic evolution of the heatsink temperature when an RMS current step reference is applied to the VSC.

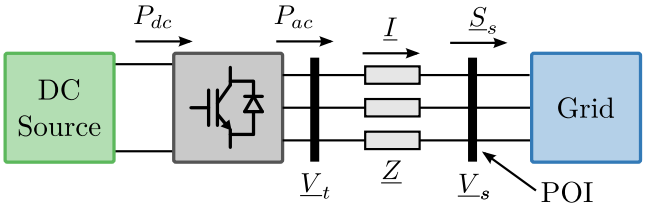

Fig. 6. Converter connected to the grid through a filter.

$$\mathbf{A} = \begin{bmatrix} 1 & I_1 & I_1\alpha_1 & I_1^2 & I_1^2\alpha_1 \\ 1 & I_2 & I_2\alpha_2 & I_2^2 & I_2^2\alpha_2 \\ 1 & I_3 & I_3\alpha_3 & I_3^2 & I_3^2\alpha_3 \\ \vdots & \vdots & \vdots & \vdots & \vdots \\ 1 & I_n & I_n\alpha_n & I_n^2 & I_n^2\alpha_n \end{bmatrix} \tag{9}$$

$$\mathbf{y}_x = \begin{bmatrix} a_x & b_x & c_x & d_x & e_x \end{bmatrix}^T \tag{10}$$

$$\mathbf{b}_x = \begin{bmatrix} P_x(I_1,\alpha_1) & P_x(I_2,\alpha_2) & \cdots & P_x(I_n,\alpha_n) \end{bmatrix}^T \tag{11}$$

The parameters are obtained by solving a linear least-squares problem which can be formulated as follows:

$$\min \left\|\mathbf{A}\mathbf{y}_\mathbf{x} - \mathbf{b}_\mathbf{x}\right\|_2 \quad x = \{i, d\} \tag{12}$$

4. Thermal model initialization

A key aspect of any electromechanical model is to define a feasible initial state before doing a small signal analysis or time domain simulations. This process, known as *backward initialization* [25], has to be extended to the thermal model introduced in this paper. The objective of the initialization is to compute the VSC power losses and temperatures of IGBTs, diodes and heatsink. The initialization of grid-connected VSC is usually based on the solution of the power flow, that yields the voltage phasor $\underline{V}_s$ at the point of interconnection (POI) given the injected VSC complex power $\underline{S} = P + jQ$, as shown in Fig. 6. Then, it is possible to compute the current through the AC coupling filter from:

$$\underline{I} = \left(\frac{\underline{S}_s}{3\underline{V}_s}\right)^*, \tag{13}$$

and the VSC voltage considering that Z is the impedance of the AC coupling filter:

$$\underline{V}_t = \underline{V}_s + \underline{I}\,\underline{Z}, \tag{14}$$

For the computation of α, both the modulation index and the power factor are required. The former parameter is derived by relating the peak value of the AC voltage with the DC bus voltage:

$$m = \frac{2\sqrt{2}V_t}{V_{dc}}, \tag{15}$$

Table 1
Characteristics of the VSCs.

Parameter	S-VSC	M-VSC	L-VSC
Manufacturer	Semikron	Infineon	ABB
Model	SKiiP25AC12F4V1	FF800R17KE	5SNA1500E33030
V_{ac} (V)	400	400	1100
V_{dc} (V)	750	800	2200
I (A)	45	650	1500
S (kVA)	30	500	3000
f_{sw} (kHz)	20	10	1
T_a (°C)	40	40	25

On the other hand, the power factor is computed by considering the phase angle difference between the VSC voltage, $\underline{V}_t = V e^{j\theta_t}$, and the VSC injected current, $\underline{I} = I e^{j\theta}$, as follows:

$$\cos\varphi = \cos\left(\theta_v - \theta\right). \tag{16}$$

The IGBT and diode power losses are computed form (5) and (6), considering steady-state conditions ($\Theta = 1$). The initial heatsink temperature, T_s^{ss} is computed by means of (4) and, after that, the IGBT and diode initial temperatures can be calculated using (1) and (2), respectively. Finally, it is possible to compute the power on the VSC DC side by just applying a power balance:

$$P_{dc} = \Re(3\underline{V}_t\underline{I}^*) \pm N_h P_s, \tag{17}$$

where the power losses sign depends on the power flow direction.

Note that this backward initialization can be performed after a power flow and does not require an iterative process.

5. Model validation

This section is devoted to validating the thermal model by comparing the estimated temperatures and power losses with the corresponding values provided by the manufacturers' software tools. The section is divided into three subsections, respectively detailing the targeted VSCs where the model has been derived, the steady-state results and dynamic simulations.

5.1. Targeted VSCs

Any general-purpose model, such as the one proposed in this paper, should fit to the actual system irrespective of its operating point, rated values and manufacturer. For this reason, in order to emphasize this versatility, the thermal model has been applied to a small (S-VSC), medium (M-VSC) and large (L-VSC) VSC of different manufacturers, according to the details shown in Table 1. Note that the switching frequencies have been selected according to the VSC power rating. In addition, different environment temperatures have been selected to evidence that the model perfectly fits to this operating condition.

The thermal model parameters of the targeted VSCs are summarized in Table 2. It is important to highlight that different information sources have been used for obtaining those parameters, because each manufacturer provides its own tool. Semikron provides the on-line software Semisel [20] while Infineon and ABB offer their corresponding spreadsheets [21,22]. The sets of parameters have been computed using just five operating points: 15%, 60% and 100% of the rated current with $\cos\varphi = 1$ and 60%, 100% with $\cos\varphi = 0$.

5.2. Steady-state results

Figs. 7 and 8 show the power losses and temperatures corresponding to the L-VSC case (large ABB VSC), as a function of the injected AC RMS for $\cos\varphi = 1$ and $\cos\varphi = 0$ respectively. The continuous curves correspond to the values computed by the proposed thermal model, while the discrete points refer to the data provided by the manufacturer

Table 2
Thermal model parameters for the targeted VSCs.

Parameter	S-VSC	M-VSC	L-VSC
R_{th}^{i-s}	0.517	0.056	0.019
R_{th}^{d-s}	0.839	0.078	0.038
R_{th}^{s-a}	0.663	0.072	0.007
C_{th}^{s}	15.08	279.66	2855.21
a_i/a_d	1.958/0.963	0.0000/43.582	434.0125/145.245
b_i/b_d	0.324/0.027	0.508/0.280	0.559/0.594
c_i/c_d	−0.227/0.051	−0.187/0.172	−0.015/0.193
d_i/d_d	0.016/0.013	0.0004/0.0002	0.0009/0.0003
e_i/e_d	−0.011/0.014	−0.0003/0.0002	−0.0005/0.0002

simulation tool. The operating points used for adjusting the model parameters have been highlighted in the figures, using bigger discrete markers. It can be observed that the power losses and temperatures of IGBT, diode and heatsink fit almost perfectly in all the operational range for both power factors.

This good matching between the proposed thermal model results and manufacturer data is achieved for different power factors, not only those used to tune the model parameters, $\cos\varphi = 1$ and $\cos\varphi = 0$ in this application. This fact can be observed in Fig. 9, where power losses and temperatures are provided for the S-VSC and M-VSC operating at $\cos\varphi = 0.8$ inductive. Again the analysis of this figure clearly shows that the fit is almost perfect, which highlights the robustness of the thermal model against different operating conditions.

5.3. Dynamic results

This section analyzes the dynamic behavior of the proposed thermal model with varying operating conditions, involving changes of AC RMS injected current, modulation index and power factor. For this purpose, the large ABB VSC is chosen, and the results are shown in Fig. 10. As in the case of the steady-state analysis of the previous section, the continuous curves corresponds to the thermal model results while discrete markers are manufacturer data. These data have been obtained from the available manufacturer tool, which allows the simulation of 10 different operating points with a total simulation time of 180 s. Therefore, several simulations have been sequentially run to obtain the results depicted in Fig. 10. The final heatsink temperature of a simulation period is used as initial temperature for the next one.

The simulation starts with a no-load condition and a steady-state heatsink temperature of 27°C, which is slightly above the environment temperature (25°C) because of the IGBT and diode losses. Note that the semiconductor switches incur in power losses just by being energized from the DC bus, even in absence of injected current, which is considered in the power losses model through the parameters a_i and a_d. At the time instant $t = 10\,\text{s}$, a step change is applied to the current, up to 1 p.u. with $\cos\varphi = 0.8$. Note that, considering the existing POI voltage, a modulation index $m = 0.8$ is required. It is worth noting also the different dynamic evolution of the IGBT and diode temperatures, with respect to the heatsink one. The current step affects directly the IGBT and diode temperatures, due to the reduced time constant of the heat transfer across the junction-case-heatsink circuit. Conversely, the heatsink temperature follows a slow first-order dynamics with similar time constant to those analyzed in electromechanical simulations.

The power losses are not only affected by the AC RMS current but also by the modulation index and power factor. For this reason, the dynamic simulation also includes step changes on these parameters in order to assess this issue. With this in mind, a step increase is simulated on the POI voltage at the time instant $t = 40\,\text{s}$, leading to a step increase of the modulating index to maintain the VSC injected current. Note that this increase in the modulation index yields a slight variation of the IGBT and diode power losses, which directly affects their temperatures but not so significantly the heatsink temperature. The influence of the

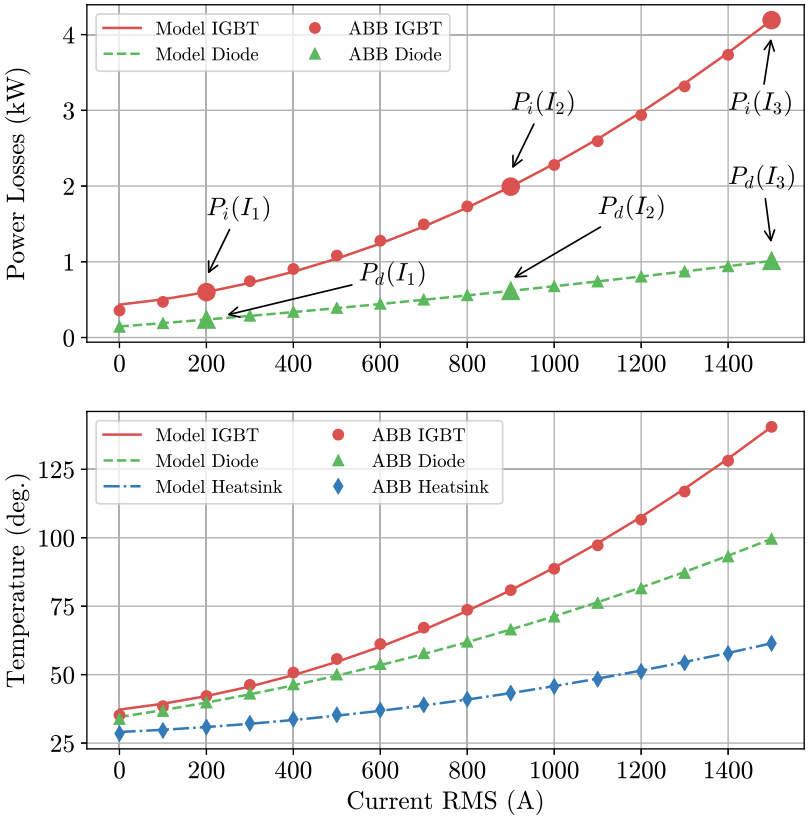

Fig. 7. L-VSC case: Power losses and temperatures with the proposed thermal model and manufacturer data with $\cos\varphi = 1$.

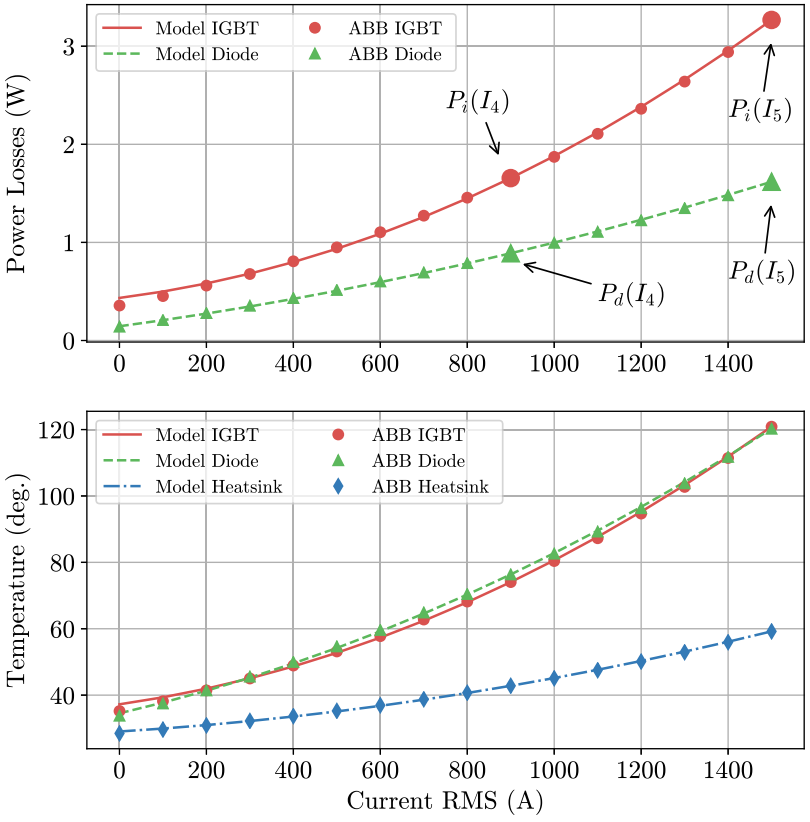

Fig. 8. L-VSC case: Power losses and temperatures with the proposed thermal model and manufacturer data with $\cos\varphi = 0$.

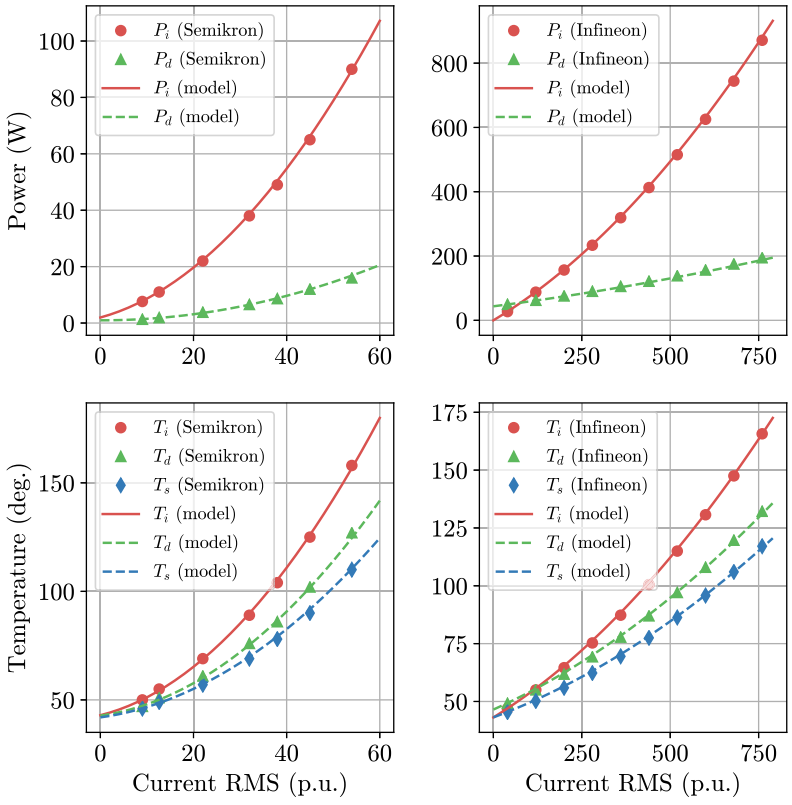

Fig. 9. M-VSC and S-VSC cases: Power losses and temperatures with the proposed thermal model and manufacturer data with $\cos\varphi = 0.8$.

power factor is analyzed at the time instant $t = 100\,\text{s}$, where a step change from $\cos\varphi = 0.85$ to $\cos\varphi = 0$ is performed. At the same time instant, the POI voltage is decreased to its original value and, therefore, the corresponding modulation index. Note that this change implies a redistribution in the IGBT and diode currents (higher current for the diode), which immediately translates to their internal temperatures. The next step change at $t = 120\,\text{s}$ corresponds to a decrease of the AC current, considerably reducing the VSC power losses and therefore its temperatures. Finally, at the time instant $t = 160\,\text{s}$ the power factor is changed to $\cos\varphi = 1$, which modifies the current sharing between the IGBT and diode just in the opposite fashion as in the previous case, therefore increasing the IGBT power losses.

The dynamic simulation reveals that the developed thermal model perfectly reproduces the VSC thermal behavior, which fits the data provided by manufacturers in their corresponding dynamic simulation software. This matching is achieved even with operating points quite different from those used in the estimation of the thermal model parameters. It is worth noting that the model exactly reproduces not only the temperature evolution but also the IGBT and diode power losses. In this regard, it is interesting to highlight the dynamic evolution of the IGBT and diode power losses, which do not exactly follow the current steps because, according to the thermal model of (5)-(6), the IGBT and diode power losses also depend on the temperature dynamics.

6. Conclusions

This paper has presented a methodology for analyzing the thermal behavior of VSCs in electromechanical simulations. A thermal domain is introduced where two different dynamics have been identified. The fast dynamics corresponds to the evolution of the temperatures of IGBT and diode junctions and the corresponding cases, while the slower one refers to the heatsink temperature. A proposal is made to simplify the fast dynamics, which reduces to a set of algebraic equations. Conversely, the slower dynamics has been fully represented by a first-order thermal model. The model has been validated with VSC from different sizes and manufacturers with accurate results both in steady-state and dynamic conditions. The discrepancies between the temperatures and power losses estimated by the proposed thermal model and the ones provided by the manufacturer are negligible, even for operating points far away from the ones used for the estimation of the model parameters.

To the best of the authors' knowledge, there is no other method in the specialized literature dealing with the integration of thermal models in electromechanical simulations. This simplification allows the evolution of all VSC temperatures to be analyzed with the larger simulation steps customarily used in electromechanical simulation programs. Therefore, the assessment of the VSC thermal behavior is extraordinarily simplified since it is possible to address the electromechanic and thermal problems simultaneously without the need of applying a tedious iterative process using different simulation platforms. Moreover, the paper has also provided a methodology for computing all the thermal model parameters from the available manufacturer data in a straightforward way.

The proposed thermal model opens new research lines dealing with the incorporation of the thermal limits in the VSC control algorithms rather than using the conservative steady-state rated AC RMS currents. This may allow, for instance, to transiently overload the VSC, which may be useful in the new power system paradigm with a massive penetration of renewable energies, where ancillary services such as inertia and primary frequency response are required to contribute to the system stability. The incorporation of the thermal model to the control algorithm may broaden the transient operational area of the VSC-based generators, providing an extended flexibility to the power system.

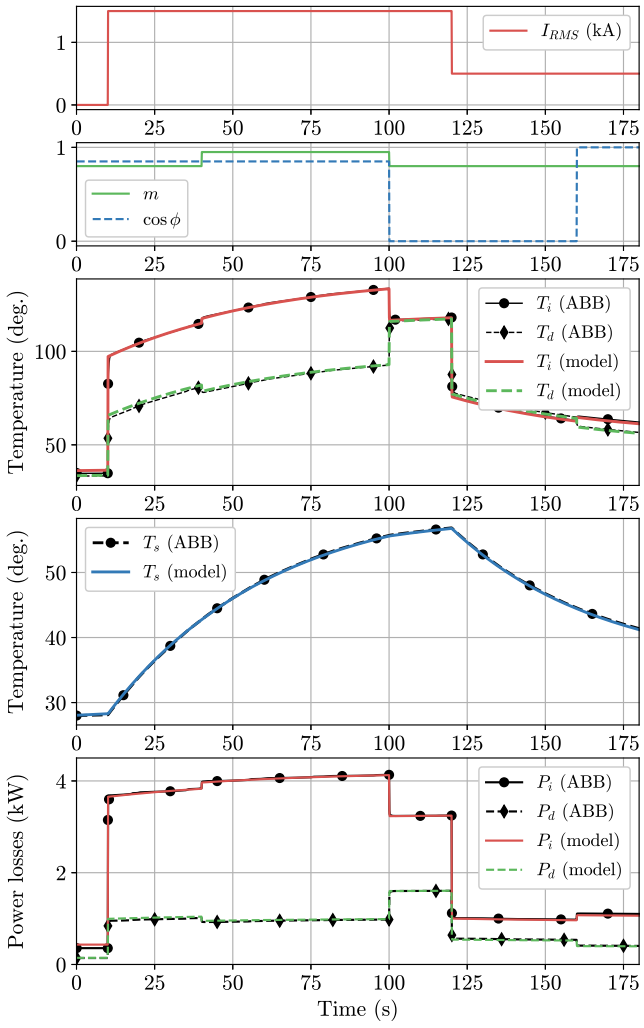

Fig. 10. Dynamic behavior of the proposed model.

Declaration of competing interest

The authors declare that they have no known competing financial interests or personal relationships that could have appeared to influence the work reported in this paper.

Data availability

All the used data are within the paper.

Acknowledgments

The authors would like to thank the funding through the grant PID2021-127835OB-I00 by MCIN/AEI/10.13039/501100011033 and "ERDF A way of making Europe". The authors would like also to acknowledge the support of the project PID2021-124571OB-I00.

References

[1] Maza-Ortega JM, Acha E, García S, Gómez-Expósito A. Overview of power electronics technology and applications in power generation transmission and distribution. J Mod Power Syst Clean Energy 2017;5(4):499–514. http://dx.doi.org/10.1007/s40565-017-0308-x.
[2] World energy outlook 2018. International Energy Agency; 2018.
[3] Tsili M, Papathanassiou S. A review of grid code technical requirements for wind farms. IET Renew Power Gener 2009;3(3):308–32. http://dx.doi.org/10.1049/iet-rpg.2008.0070.
[4] CENELEC. Requirements for generating plants to be connected in parallel with distribution networks - part 1: Connection to a LV distribution network, EN50549-1:2015.
[5] Martínez J, Kjær P, Rodriguez P, Teodorescu R. Comparison of two voltage control strategies for a wind power plant. In: 2011 IEEE/PES power systems conference and exposition. 2011, p. 1–9. http://dx.doi.org/10.1109/PSCE.2011.5772470.
[6] Malamaki K, Demoulias C. Estimation of additional PV converter losses operating under pf ≠ 1 based on manufacturer's data at pf=1. IEEE Trans Energy Convers 2019;34(1):540–53. http://dx.doi.org/10.1109/TEC.2019.2893065.
[7] Zhong Q, Weiss G. Synchronverters: Inverters that mimic synchronous generators. IEEE Trans Ind Electron 2011;58(4):1259–67. http://dx.doi.org/10.1109/TIE.2010.2048839.
[8] Torres M, Lopes L, Morán L, Espinoza J. Self-tuning virtual synchronous machine: A control strategy for energy storage systems to support dynamic frequency control. IEEE Trans Energy Convers 2014;29(4):833–40. http://dx.doi.org/10.1109/TEC.2014.2362577.
[9] Mauricio JM, Marano A, Gómez-Expósito A, Martinez Ramos JL. Frequency regulation contribution through variable-speed wind energy conversion systems. IEEE Trans Power Syst 2009;24(1):173–80. http://dx.doi.org/10.1109/TPWRS.2008.2009398.
[10] Kakimoto N, Satoh H, Takayama S, Nakamura K. Ramp-rate control of photovoltaic generator with electric double-layer capacitor. IEEE Trans Energy Convers 2009;24(2):465–73. http://dx.doi.org/10.1109/TEC.2008.2001580.
[11] Li X, Hui D, Lai X. Battery energy storage station (BESS)-based smoothing control of photovoltaic (PV) and wind power generation fluctuations. IEEE Trans Sustain Energy 2013;4(2):464–73. http://dx.doi.org/10.1109/TSTE.2013.2247428.
[12] Hefner AR. A dynamic electro-thermal model for the IGBT. IEEE Trans Ind Appl 1994;30(2):394–405. http://dx.doi.org/10.1109/28.287517.
[13] Myaing A, Faruque M, Dinavahi V, Dufour C. Comparison of insulated gate bipolar transistor models for FPGA-based real-time simulation of electric drives and application guideline. IET Power Electron 2012;5(3):293–303. http://dx.doi.org/10.1049/iet-pel.2011.0105.
[14] Brückner T, Bernet S. Estimation and measurement of junction temperatures in a three-level voltage source converter. IEEE Trans Power Electron 2007;22(1):3–12. http://dx.doi.org/10.1109/TPEL.2006.886651.
[15] Rajapakse A, Gole A, Wilson P. Electromagnetic transients simulation models for accurate representation of switching losses and thermal performance in power electronic systems. IEEE Trans Power Deliv 2005;20(1):319–27. http://dx.doi.org/10.1109/TPWRD.2004.839726.
[16] Luo H, Chen Y, Sun P, Li W, He X. Junction temperature extraction approach with turn-off delay time for high-voltage high-power IGBT modules. IEEE Trans Power Electron 2016;31(7):5122–32. http://dx.doi.org/10.1109/TPEL.2015.2481465.
[17] Gorecki K, Zarebski J, Gorecki P, Ptak P. Compact thermal models of semiconductor devices- a review. Int J Electron Telecommun 2019;65(2):151–8. http://dx.doi.org/10.24425/ijet.2019.126295.
[18] Gorecki K, Zarebski J, Gorecki P. Nonlinear compact thermal model of the IGBT dedicated to SPICE. IEEE Trans Power Electron 2020;35(12):13420–8. http://dx.doi.org/10.1109/TPEL.2020.2995414.
[19] Azar R, Udrea F, Ng W, Dawson F, Findlay W, Waind P, et al. Advanced electrothermal spice modelling of large power IGBTs. IEE Proc - Circuits Dev Syst 2004;151(3):249–53. http://dx.doi.org/10.1049/ip-cds.
[20] Semikron. Thermal resistance of IGBT modules - Specification and modelling. Tech. rep. Semikron; 2014.
[21] Infineon. Thermal equivalent circuit models. Tech. rep. Infineon; 2008.
[22] ABB. Applying IGBTS. Tech. rep. ABB.
[23] Wang X, Wang X, Yuan X. An optimal dc bus voltage control method to improve the junction temperature of IGBTs in low speed operations of traction applications. In: 2016 IEEE 2nd annual southern power electronics conference. 2016, p. 1–6. http://dx.doi.org/10.1109/SPEC.2016.7846201.
[24] Sundaramoorthy V, Bianda E, Kamel M, Riedel G, Nistor I. Online junction temperature estimation for IGBT modules with paralleled semiconductor chips. In: 7th IET international conference on power electronics, machines and drives. 2014, p. 1–5. http://dx.doi.org/10.1049/cp.2014.0406.
[25] Milano F. Power system modelling and scripting. Springer; 2010.
[26] Murthy K, Bedford R. Transformation between foster and cauer equivalent networks. IEEE Trans Circuits Syst 1978;25(4):238–9.
[27] Gorecki K, Gorecki P, Zarebski J. Measurements of parameters of the thermal model of the IGBT module. IEEE Trans Instrum Meas 2019;68(12):4864–75. http://dx.doi.org/10.1109/TIM.2019.290014.
[28] Ma X, Sun H, Wang H, Zhao J, Yang Y. Experiment-based investigation of thermal cross-coupling of chips in high-power IGBT modules. In: 2020 PCIM Asia international exhibition and conference for power electronics, intelligent motion, renewable energy and energy management. 2020, p. 1–7.